Stainless Steel 304 Sheets Modelling of Bending Properties Welded by Tungsten Inert Gas Welding Process

Hadyan Ali Alajmi[1],
[1]Specialist Trainer (B) in Public Authority for Applied Education and Training,
The University of Arab Academy for Science, Technology and Transport

Meshal Essa Essa[2]
[2]Specialist Trainer (B) in Public Authority for Applied Education and Training,
ASTM International University, Eygpt

Abstract:- This study was conducted in order to examine the effect of the welding current and the gas pressure of argon on the welded joints' characteristics, especially the bending properties. Welding using the Tungsten inert gas (TIG) is conducted on 304-stainless-steel sheets based on the probable values of currents and welding gas pressures. Accordingly, the impact of both parameters on the max bending force (MBF) value of the welded joints by TIG was understood. Using the Design of the experiment (Version.10) denoted by (DOE), the experiment's design matrix was determined based on the input factors values. Also, a mathematical and empirical model was attained based on a technique known as Response-Surface-Methodology (RSM). The proposed model dealt with the effect of the prementioned welding parameters on the welded zone's MBF value, in which the parameters are the gas pressure and the current values. Finally, verification of the model adequacy was performed using ANOVA, which is the analysis of variance.

Keywords: Welding, Gas Pressure of Argon, Bending Properties, Tungsten Inert Gas, Max Bending Force, Response-Surface-Methodology.

I. INTRODUCTION

The TIG is a crucial welding process in which a non-consumable tungsten electrode is used while welding; also, an inert gas is used for arc shielding. TIG is primarily utilized for welding some materials, such as stainless steel, that are difficult to be welded in the ordinary procedure. The TIG welding quality is distinguished by the geometry of the welding pool, which the welding pool geometry is essential for evaluating the mechanical properties of the welding area. Several features characterize the welding pool, such as the front breadth, the back breadth, the front height, and the back height. The electric arc strikes the base material. This arc is employed by the tungsten electrode covered with an inert gas. The base material (plates made of 304-stainless steel) will be melted because of the created heat from the produced arc. Accordingly, the base material will be joined. An A.C. welding machine is used as a power source. Also, A valve meter is used to control and monitor the flow rate regarding the shielding gas, noting that argon is used as a shielding gas (Juang & Tarng, 2002). Figure 1 represents the basic sketch of the TIG welding process.

Moreover, several parameters affect the welding process using TIG, such as the flow rate, arc gap, welding speed, welding current, etc. Therefore, the proper selection of these parameters will enhance the welding quality (Juang & Tarng, 2002).
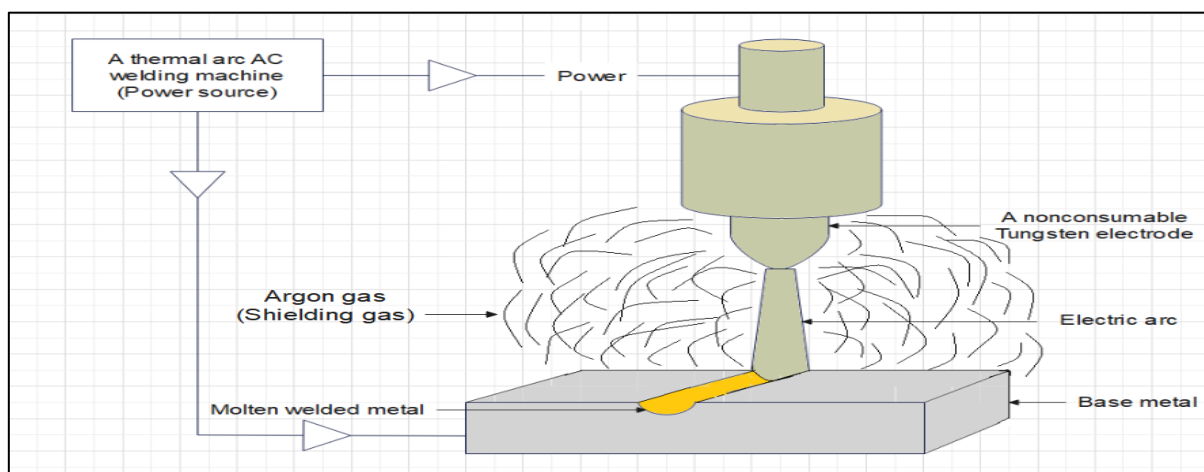

Fig 1 The basic Sketch of the TIG Welding Process

II. LITERATURE REVIEW

Due to the varying properties of the materials/items to be joined, the welding process is considered difficult as the thermal, chemical, and mechanical properties are different when these materials are subjected to certain welding conditions. (Kesava, 2021) Studied the welding process of two different plates of steel (AISI 310 and AISI 304) using the TIG welding process. This study considered several input parameters, including the gas flow rate, feed rate, and welding current. At the same time, the responses are the MBF and the strength. Central-Composite-Design adopted the Response-Surface-Method to conduct 31 experiments for four factors and five levels to measure the impact strength, tensile strength, and MBF. Also, at 95% confidence, ANOVA was conducted.

(Kumar & Shahi, 2011) Explored the heat impact as an input value on the mechanical characteristics and the microstructure of the joints produced by joining two plates of 304 stainless steel material using a gas tungsten arc. Three heat input values were studied: low, medium, and high heat values. The joints produced at low heat levels show a greater value of the ultimate tensile strength (UTS) compared to those produced at the high and medium heat input values. Also, the grains were coarser as the heat increased. Also, the inter-dendritic spacing and the dendrite length within the welding area increase as the heat input value increases. (Saha, et al., 2019) Several parameters affect the welding pool geometry, such as heat, voltage, current, arc speed, and travel speed. While conducting the experimental work, the welding process was performed on E350 structural steel alloy at different combinations of the input values with increasing the quantity of heat input from 0.35 kJ/mm to 0.75 kJ/mm. According to the observations, the breadth of the welded bead increased linearly as the heat input value increased. However, the heat input does not affect the penetration depth. The regression analysis obtained the relationship that combined the heat input value with the bead's geometrical parameters. Thus, an agreement is achieved between the experimental data and the regression models. Furthermore, wider beads are obtained when higher heat is applied, noting a slight change in reinforcement and penetration is noted.

The 304-stainless steel sheet's welding behaviour was studied by (Zuhailawati et al., 2016). (Zuhailawati, et al., 2016) Investigated the microstructure and strength of the joints, in which the composition analysis was conducted for the ER308 filler rod and the stainless-steel plates using SEM-EDX and X-ray fluorescence. Mathematical relations for connecting the input parameters with responses were developed using the RSM. The input parameters were the filler size, the shielding gas flow rate, and the welding current. At the same time, the response was the UTS. This process is performed to determine the best values that ensure the desired quality of the welded joints. A good agreement was achieved using the developed models. Therefore, the welding parameters limits are predicted to achieve the desired quality and responses. Weaker joints are obtained when employing low current inputs; however, higher current

values lead to a finer microstructure of higher tensile strength. Also, implying more minor fillers lead to a better tensile strength value since the high heat values are utilized for melting the large filler and overheating the base material. A drop in tensile strength is noted when employing high flow rates.

(ÇALIGÜLÜ , et al., 2012) Concluded that the welding speed also impacts the structure of the welded area. Several heat input values with varying welding speeds were applied on 304-Austenitic stainless-steel plates. The generated welded areas were checked and examined using XRD, EDS, SEM, and optical microscopy. The welding zone breadth was observed to become significantly thinner based on increasing the welding speed. Furthermore, the breadth became wider as the heat value increased. The tensile strength values agree with these findings. (Babbar, et al., 2019) Concluded that the tensile strength values obtained by the A-TIG welding are better. When the current, speed, and flow rate are 110 Amp, 82 mm/min, and 14 L/min, respectively, the max value of DOP obtained is 8.283 mm.

(Naik & Reddy, 2018) Discussed several parameters regarding enhancing and optimizing the stainless-steel tensile strength using TIG depending on ANOVA and Taguchi method. An orthogonal array is conducted to define the issues regarding the welding process. Then, errors will be minimized in predicting the output values within the neural network. In this research, the hardness, tensile strength, and welding depth were the studied responses based on several input parameters, including time, speed, current, gas flow rate, electrode diameter, and oxide fluxes variation. (Naik & Reddy, 2018) Observed that ANOVA and Taguchi methods are effective in enhancing welding quality. As it is beneficial, (Kumar, et al., 2007) found that several advantages are achieved by the pulsed current compared to the traditional continuous current within a TIG welding process. The pulsed current can enhance the mechanical properties of the welded area since it refines the grains within the fusion area.

(Ogedengbe, et al., 2018) Aims to examine the impact of welding speed, gas flow rate, and current on the welded area's mechanical characteristics and microstructure. The gas tungsten welding process was performed on low-carbon steel and AISI 304 stainless steel. (Ogedengbe, et al., 2018) Noticed that the studied input parameters substantially influence the welded zone's UTS values. The current impact was noticed to be the highest, while the impact of the gas flow rate was noticed to be the lowest. Furthermore, the penetration and the grain size contribute to the tensile strength. Also, the tensile strength increases as the welding speed and current decrease. All the studied factors with the welding speed contribute to the hardness.

III. METHODOLOGY

➢ *Materials Selection, Samples Preparation, and Welding Process*

An alloy made of 304-stainless steel sheet was utilized in this work. The alloy was purchased from the market with a thickness of $2.0\ mm$. Table 1 summarizes the chemical composition of the treated alloy, in which these properties are mentioned according to the ASTM standards. The welding samples were cut using an electronic machine to achieve the required dimensions of $(200 \times 100)\ mm^2$. Finally, the sheet edges were ground; so that the two mounted specimens had no in-between gaps.

Table 1 The Chemical Elements exist within a 304-Stainless Steel Alloy

Name of element	Cr	Ni	Mn	Si	N	C	P	S	Mo
Percentage of weight	18.0	8.0	2.0	0.75	0.1	0.08	0.045	0.03	00

A skilled technician was responsible for the welding process. As the sheets must be welded together in one alignment, the sheets were firmly fixed on the welding board during welding. In this work, the TIG 160 machine was used to accomplish the welding process, in which its technical data are presented in Table 2.

Table 2 Welding Machine Data

Technical data regarding the welding machine	Circuit Voltage	Power Factor	Circuit Power	The diameter of Tungsten electrode and welding filter rod
Data	65-80 v	0.69	30 W	1.6 mm

The inert gas used in this experimental work is argon gas which could be adjusted manually using an organizer. Due to its suitability with the material of the welding samples (304-stainless steel), the 304-welding filler was used. Moreover, to better understand the welded joints' quality in terms of the best quality and welding efficiency, two parameters will be investigated: the current and the pressure of the welding gas, since the high mechanical properties indicate the high efficiency of the welding process.

➢ *Experimental Design Matrix*

A mathematical model is made during the DOE procedure to measure the response to gas pressure and current parameters. The response will be measured by investigating the MBF. Moreover, ANOVA is used for performing a statistical analysis to determine the importance of the model; also, to find the optimal output values at optimal input values using numerical optimization where the MBF is the desired output and the parameters and the input values. Then, to validate the results, the confirmation test will be performed at optimal conditions. So, the error will be calculated based on the variation between the hypothetical and experimental results. The input parameter's matrix is built using DESIGN EXPERT computer programming, in which the response surface methodology, denoted by (RSM), is used in this computer programming. Some previous research was used to determine the values of the input parameters to be employed in this experimental work. Table 3 involved factors within two levels.

Additionally, RSM experiments according to two input parameters (the current and gas pressure) to find four outputs with four and five axial and central points, respectively, using a central rotatable composite design. Thirteen experimental runs were conducted based on the experimental matrix design. Each parameter experiences two coded levels of +1 and -1, as every code is layered with an actual value tantamount. Table 3 presents the input parameters with the high and low levels.

Table 3 High and Low Levels of the Input Parameters Utilized with Coding

Parameter	High Level (+1)	Low Level (-1)
Gas Flow Pressure (kgf/cm2)	13	15
Current (A)	80	100

➢ *Testing The Mechanical Characteristics*

- *Tensile Test*

The tensile test was done for the samples based on the ASTM standards using the Tinius Olsen machine of 5 kN max capacity. Furthermore, the samples were prepared for the tensile test using the CNC milling machine. Figure 2 represents the tensile sample geometry prepared regarding the ASEM E8-M standards. Three samples' mean value was calculated to investigate the welded joints' tensile properties. This mean value is calculated in the vertical direction corresponding to the welded line, in which the crosshead speed was maintained constant at 1 mm/min for all cases. Table 4 concludes the results regarding tensile stress.
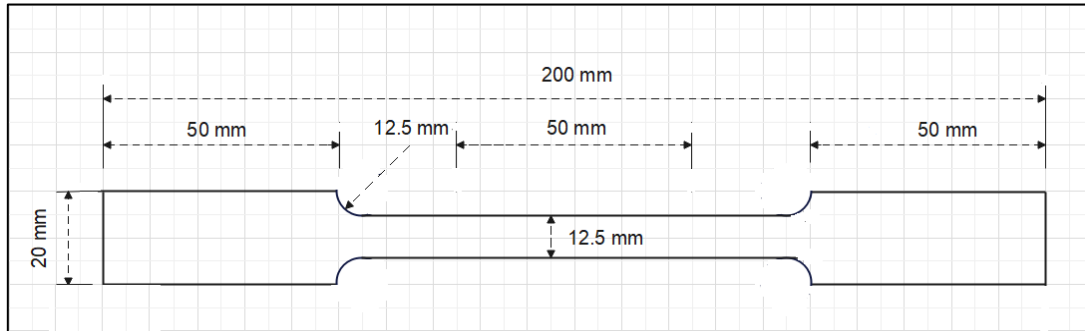

Fig 2 Rectangular Cross-Sectional Samples for Conducting the Tensile Test

Table 4 Results of Tensile Stress

Standard Number	Run Number	Ultimate Tensile Stress
1	2	353
2	8	527
3	3	715
4	1	703
5	4	606
6	7	570
7	9	313
8	6	660
9	10	694
10	13	695
11	12	715
12	5	710
13	11	711

- *Bending Test*

The bending test was conducted according to the ASTM standards (ASTM E190). Tinius Olsen machine is used for the bending test as this test was performed under (1mm/min) compression speed with no need to maintain a specific temperature (performed at room temperature). The MBF was evaluated by conducting the bending test on three points. Then, the average of the three values was calculated, in which the welding is performed in the vertical direction corresponding to the welding line, as presented in Figure 3. The bending test was conducted according to the ASTM standards (ASTM E190). Table 5 concludes the results regarding .Max. Bending Force.
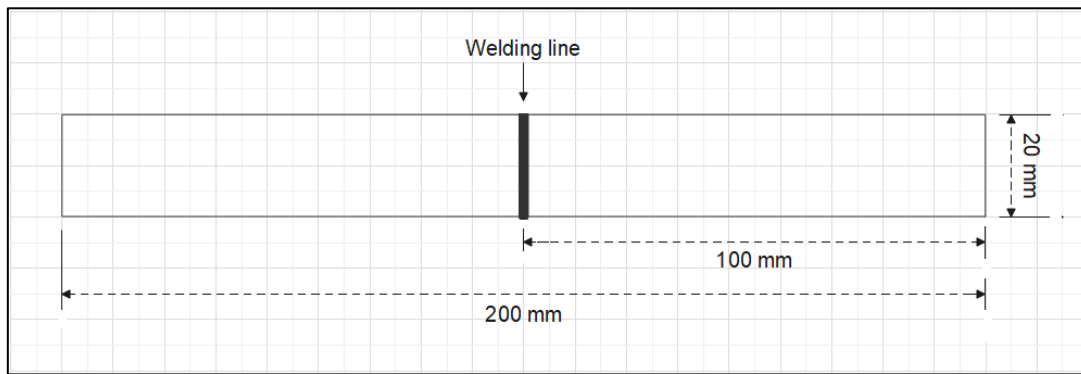
Fig 3 Bending Test Samples

Table 5 Results of Tensile Stress

Standard Number	Run Number	Max. Bending Force
1	2	360
2	8	592
3	3	683
4	1	600
5	4	589
6	7	535
7	9	485
8	6	755
9	10	487
10	13	490
11	12	587
12	5	548
13	11	565

IV. RESULTS AND DISCUSSION

➢ *Results Regarding the Tensile and Bending Tests*

A visual examination of the welding joints was performed after experimenting. The bending and tensile samples were chosen depending on the suitable parts of the welded surface. The results regarding the bending and tensile tests are represented in Table 4 and Table 5. The base material shows ($410\ N$ and $622\ MPa$) values of the MBF and the tensile strength, respectively. When the gas pressure and the current value were maintained at $16\ Kgf/cm^2$ and $90\ Amp$, respectively, the max value of the yield stress was achieved. However, the elongation and the UTS were achieved at $80\ Amp$ and $15\ Kgf/cm^2$ of both the current value and gas pressure, respectively.

As the gas pressure increases (when the current value is maintained at 90 Amp), higher values are obtained for the tensile stress. Accordingly, the gas pressure is of a significant impact on the tensile stress value, and this impact is higher when compared with the welding current impact. This observation is due to the gas protection effect that overcame the heat input impact generated by the current. Also, this observation agrees with the previous research as the tensile strength values of the 304-stainless steel plates that are joined using TIG, in which the observed values were higher than the base materials. Furthermore, low heat inputs will generate the best tensile strength values.

➢ *The Maximum Bending Force (MBF) Model*

The least square method calculates the response model in (response surface/response), in which the mean response is achieved for an MBF value. A diminutive quadratic model was analyzed to predict the MBF, in which the variance was statistically analyzed in this model using ANOVA with the backward exclusion of irrelevant coefficients. Table 6 shows the ANOVA statistical analysis generated using software for the other terms.

Table 6 ANOVA for Two Factors Interactivity Model for MBF

Stand. Dev.	45.6
Mean	559.69
C.V%	8.15
Press	44880.88
R^2	0.8541
Adjusted R^2	0.7811
Pred. R^2	0.6063

At a confidence level of 95%, the model is considered significant. This model demonstrates that the three terms of $A.B., B$, and B^2 have a higher impact on the MBF. Where AB denotes the interactivity of gas pressure and current, B denotes gas pressure, $and\ B^2$ refers to the squared gas pressure. Consequently, the equation regarding the MBF value as a function of real parameters (current is denoted by A, and the gas pressure is denoted by B) is:

$$Max. (B.F.) = -6662.92284 + (110.59167 \times A) + (243.54321 \times B)$$

$$-(7.87500 \times A \times B) + (19.20679 \times B^2)$$

Fig 4 shows the normal probability of the MBF. It is noted that residuals mostly existed in a single straight line and had a normal distribution implying the errors.
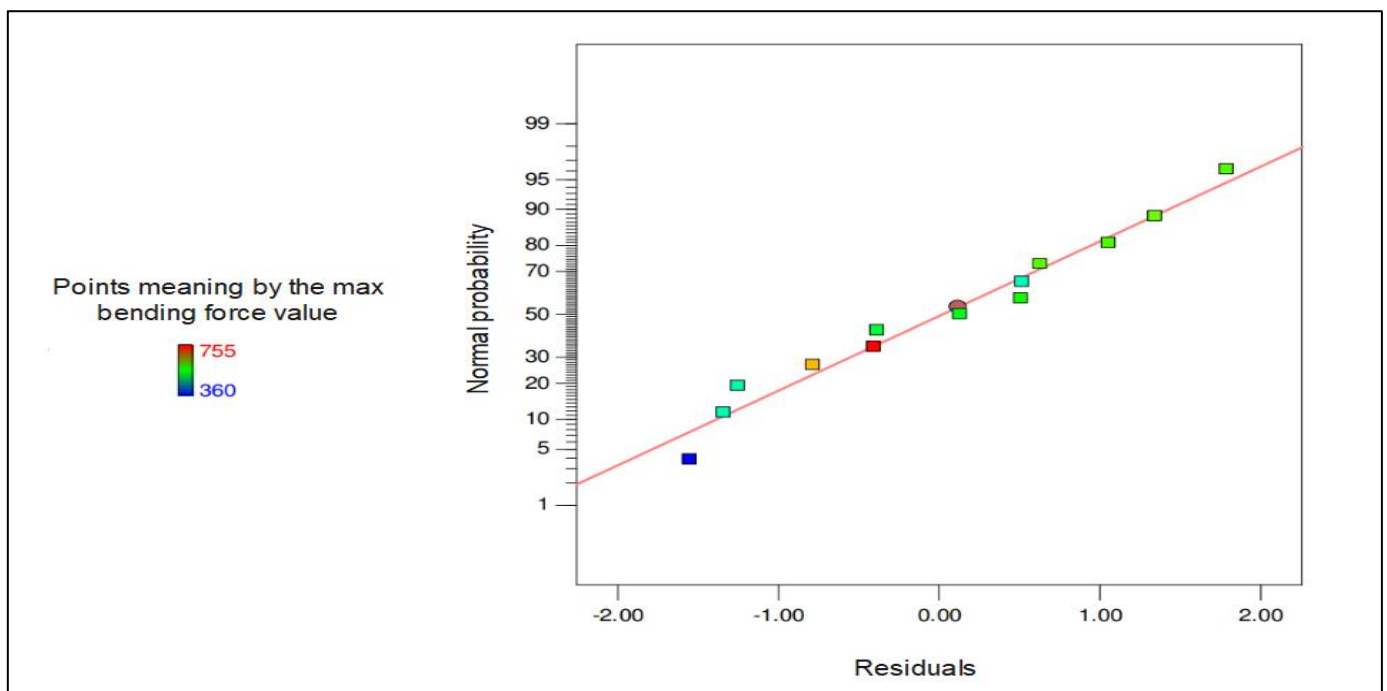

Fig 4 MBF Normal Distribution

Figure 5 represents the residuals versus the expected output values regarding the MBF. It's clear that the patterns are not obvious with unusual structure occurs, involving that the models are precise.
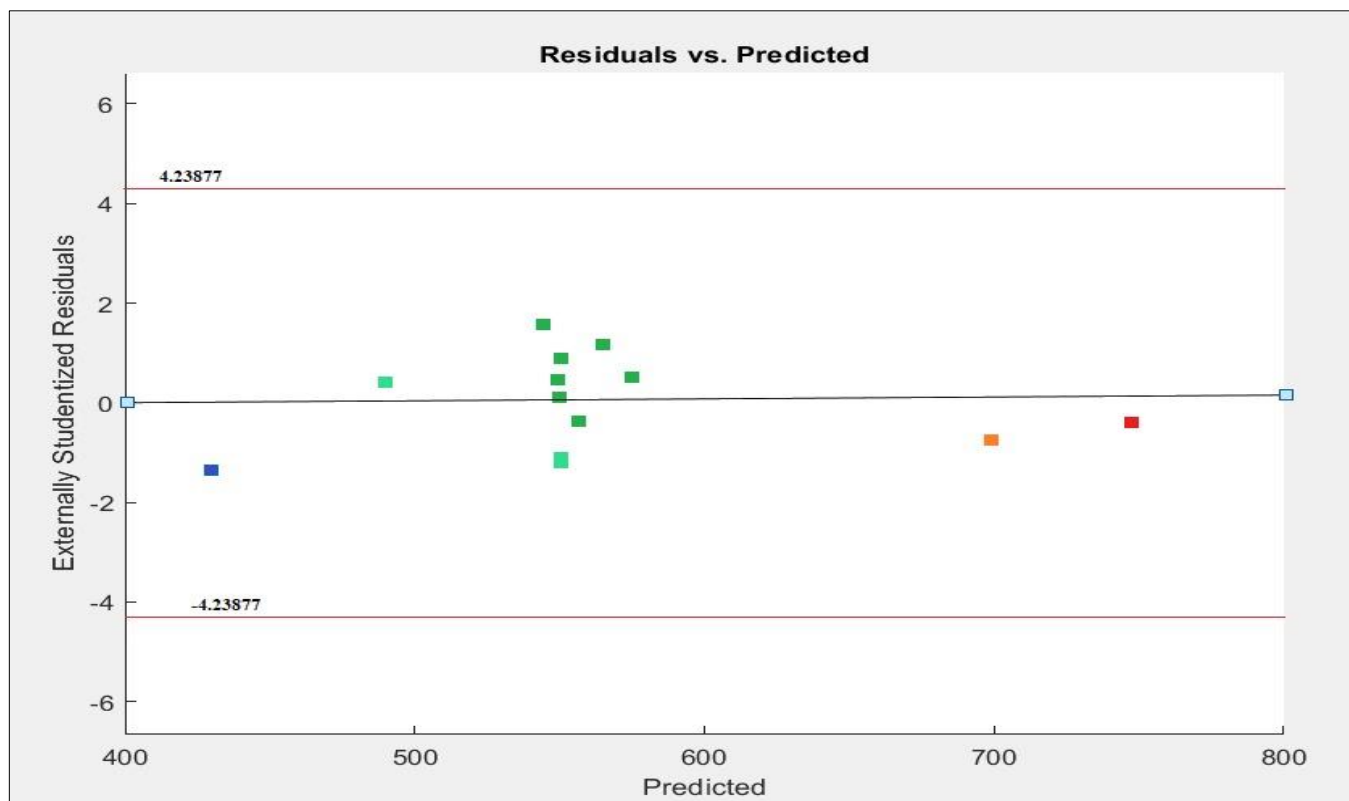
Fig 5 Residual vs Predicted Data

Figure 6 displays the MBF in terms of perturbation, which indicates the impact of current and gas pressure on the MBF. Therefore, it is observed that the gas pressure has a more significant influence on the MBF.

Figure 7 shows the outcomes of MBF in terms of perturbation. Nevertheless, Figure 8 displays the combined impact of both factors after the mean value reaches nearly the current 95 Amp.
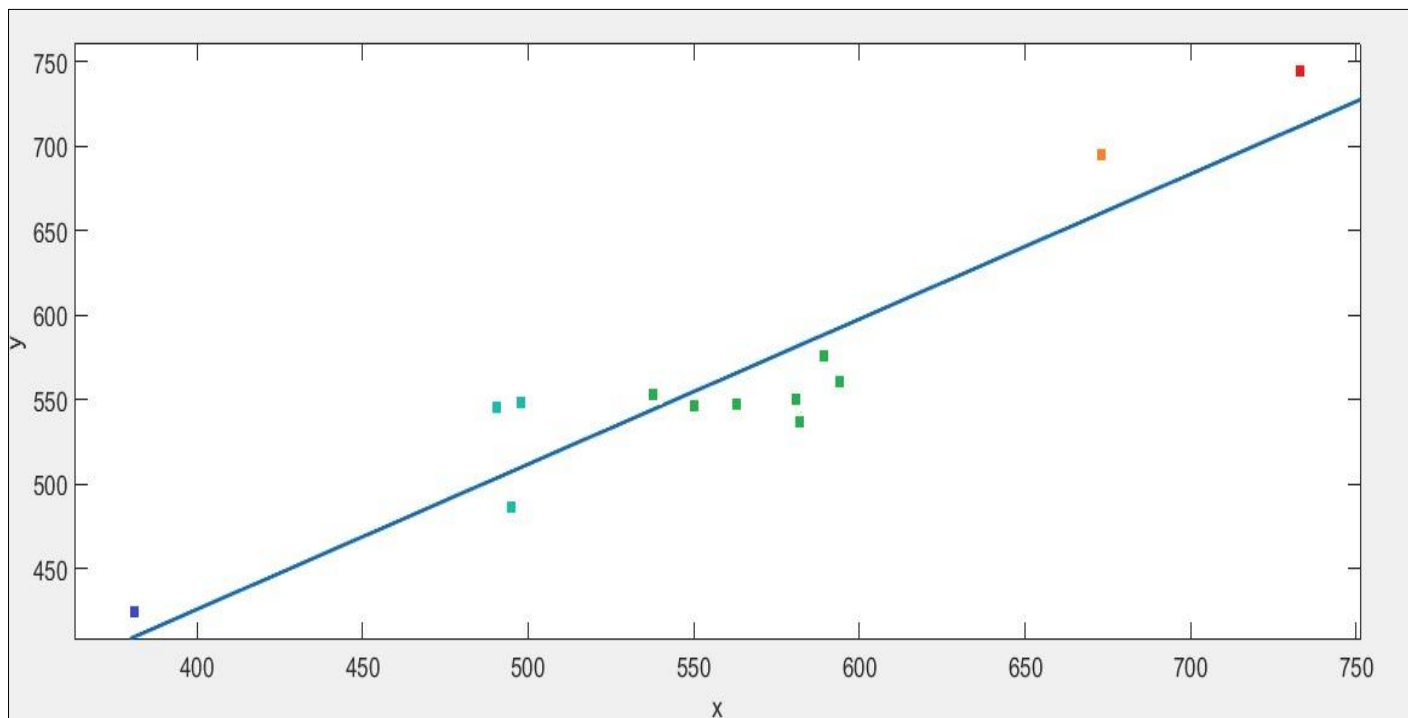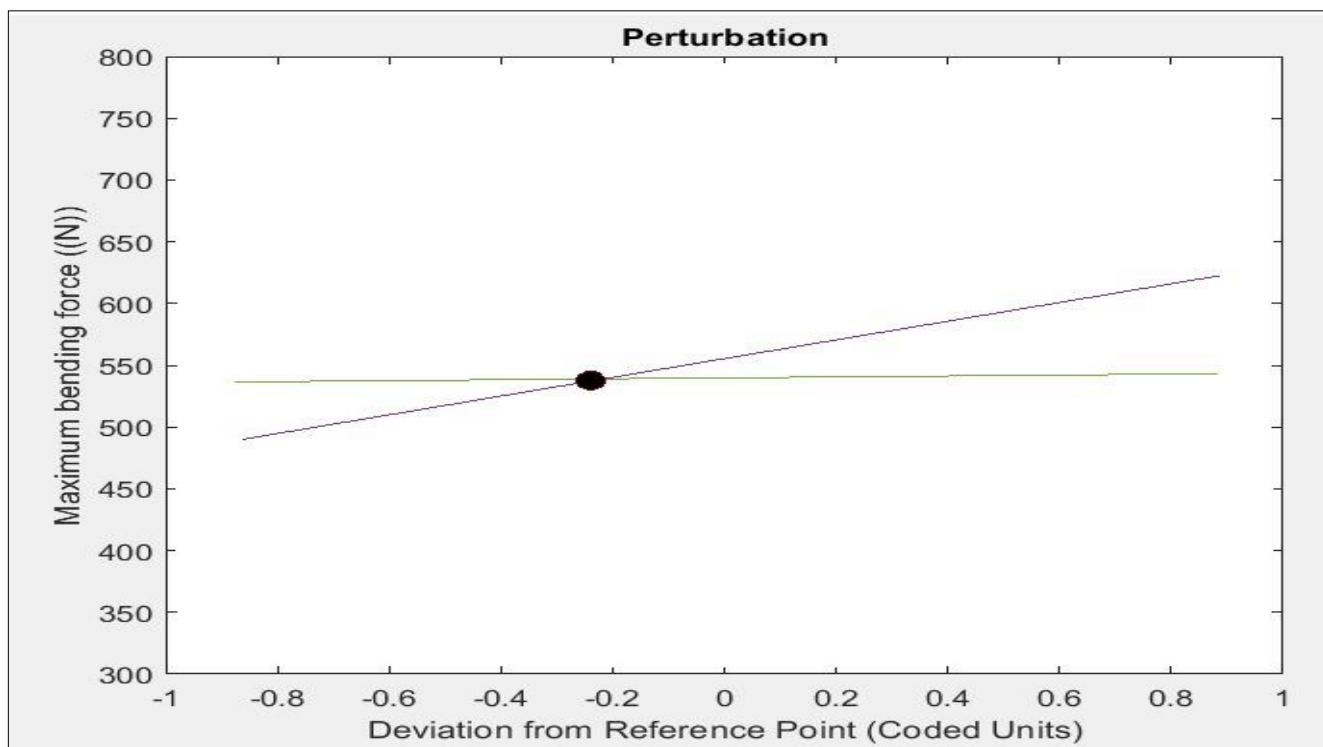

Fig 6 Predicted Vs. Real Data

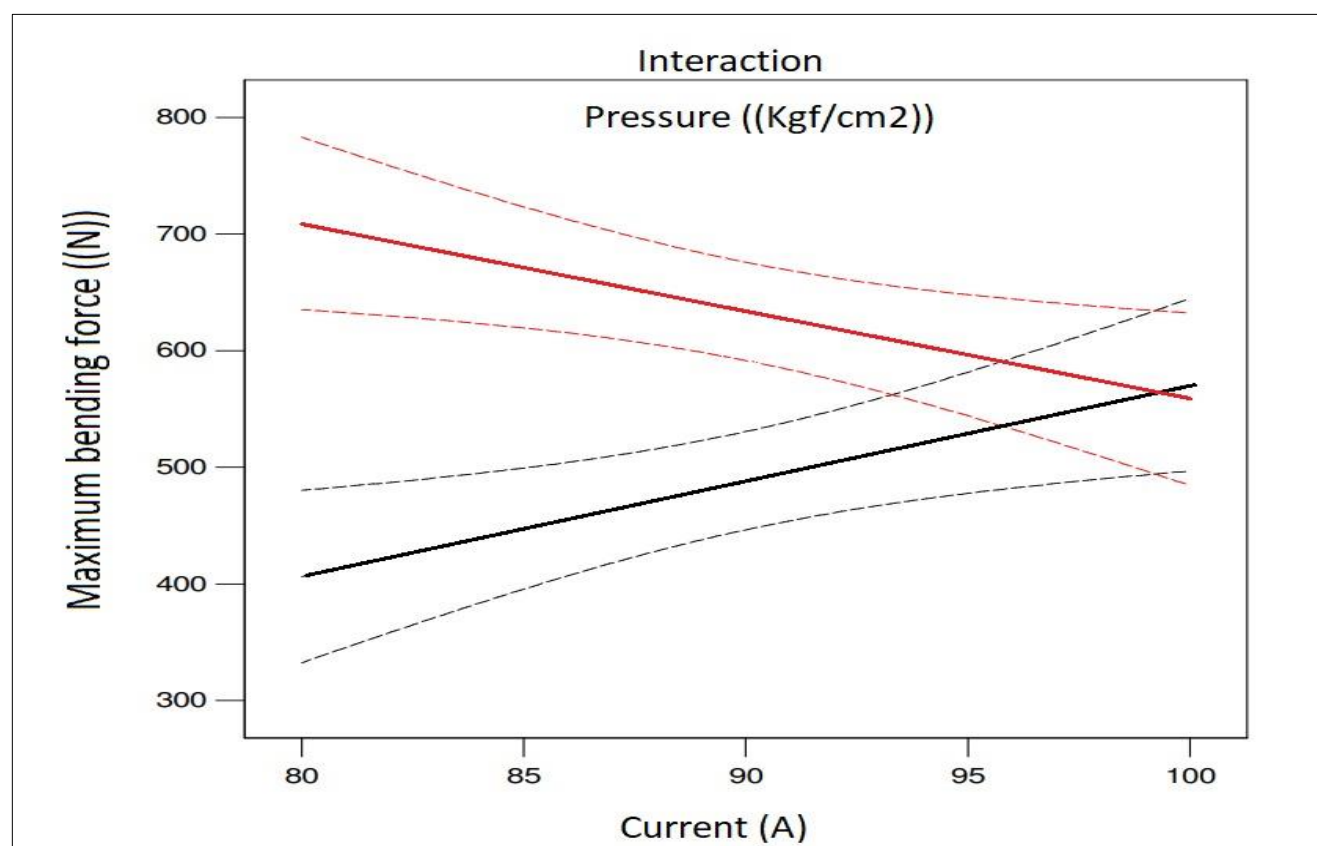Fig 7 The MBF in Terms of Perturbation

Fig 8 Interactivity Relationship between Current and Gas Pressure

Figure 9 shows the two-dimensional contour graph for the MBF in terms of current and gas pressure. Therefore, as both the current and gas pressure increase, the MBF will increase.
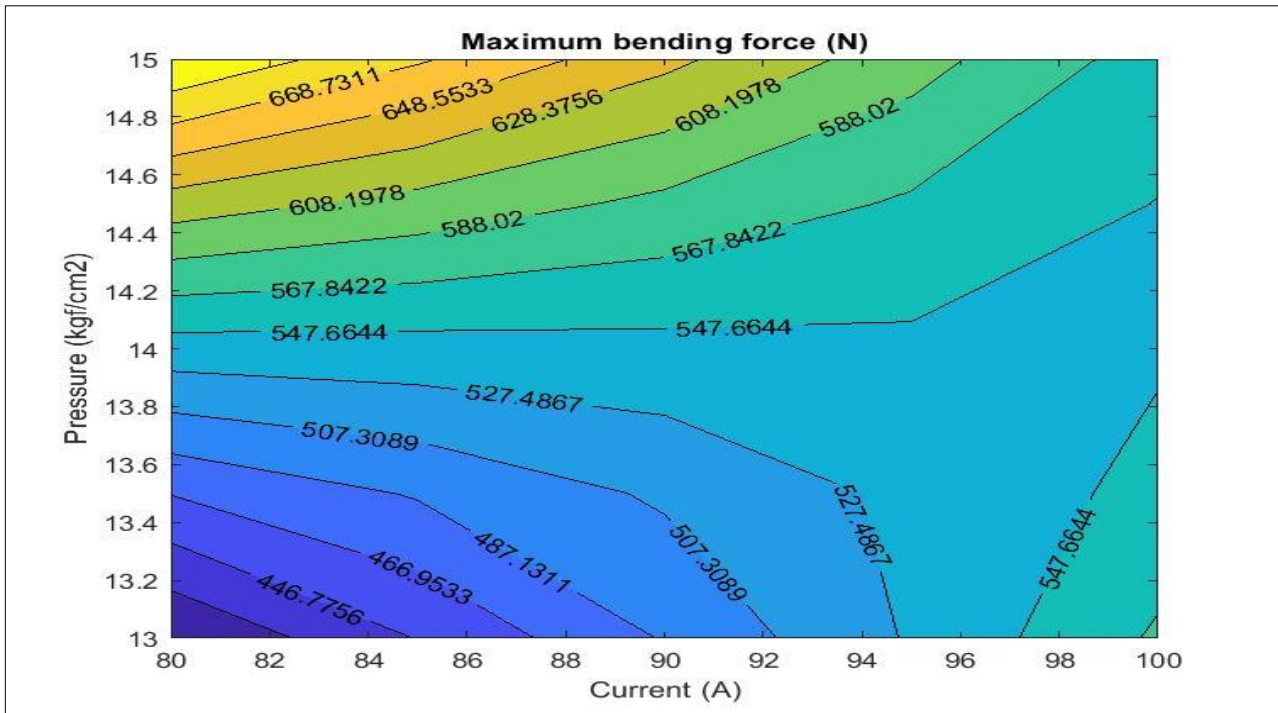
Fig 9 2-Dimensional Graph of MBF Regarding Gas Pressure and Current

It is obvious that a MBF occurs by increasing the gas pressure value at which the lower current value is 80 Amp. The force value is noted to be larger than 665 N since higher joint protection will be achieved by the influence of greater gas pressure values. However, increasing the current value (equals 100 Amp) with maintaining the gas pressure at the minimum value of 13 Kgf/cm^2 will cause a MBF larger than 560 N. This result occurred since the max values of the current led to higher heat input and consequently caused a higher thermal effect. From the outcomes above, two parameters, current, and gas pressure, impact the MBF. In addition, the pressure of a gas has more significance on the bending force than the current value when investigating these parameters individually. Figure 10 presents the interactivity between the two factors: the gas pressure and the welding current of values that approximately equals 14 Kgf/cm^2 and 95 Amp, respectively.
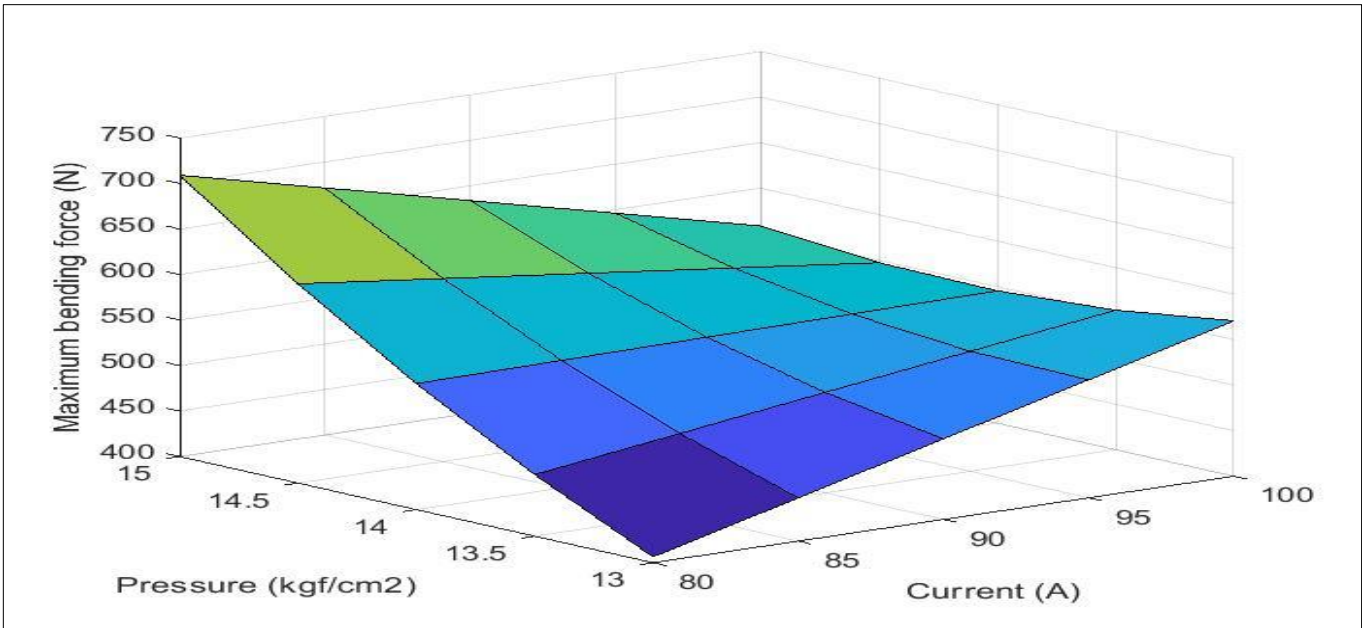

Fig 10 3-Dimensional Graph of MBF Regarding Gas Pressure and Current

The impact of these two parameters generates a lower value of the MBF, which is lower by approximately compared to the value generated separately. Figure 10 shows the 3D plot for the MBF in terms of gas pressure and current, and it proves the perception mentioned in the previous 2D graph. The growth of two parameters, gas pressure and current, will cause an increment in the value of the MBF within the parameter's max level.

➢ *MBF Optimization*

The optimal values of parameters are determined to find the needed requirements regarding the welding joints. These values are determined by the DOE optimization based on the findings of the predicted quadratic models in terms of the two parameters. In which the quadratic models are used to determine the MBF. The optimization parameter's constraints, and the output requirements' goal is presented in Table 7.

Table 7 The Optimization's Constraints

Parameter Name	Lower and Upper Limit	Lower and Upper Weight	Importance
Pressure	13-15	1-1	3
Current	80-100	1-1	3
Bending Force	360-755	1-1	3

Using numerical optimization, a recent objective function (desirability) was expected and boosted. Then, the predicted (expected) model that varies between (0 and 1) at the required goal will be modified. The optimization's essential aim was to evaluate the max result response that fits with the parameter's MBF simultaneously. The parameter constraint was utilized for the numerical optimization regarding the MBF. Also, the input parameters were chosen based on their applicable ranges, and the maximum response values were chosen.

Table 8 Input's Optimal Values and Outputs

Parameter Name	Unit	Value
Gas Pressure	Kgf/cm2	15
Current	A	80
Bending Force	N	709
Desirability	-	0884

Accordingly, as presented in Table 8, one probable solution confirms such constraints in determining the MBF values at (709 N) with a max desirability value (0.884) at the weld current optimal and gas pressure values of (80Amp) and (14 Kgf/cm^2), respectively.

➢ *Confirmation Tests*

The confirmation test was performed at the optimal gas pressure and current values to achieve better accuracy and validate the MBF values, as presented in Table 9. The mean values of the confirmation test results are concluded in Table 9 to compare the predicted and experimental results.

Table 9 Outcomes of Confirmation Tests at Optimal Conditions

Parameter Name	Unit	Value
Gas Pressure	Kgf/cm2	15
Current	A	80
Bending Force	N	683
Predicted Bending Force	N	709
Error Value	%	3.8

Therefore, after determining the predicted and experimental results of the MBF, it has been observed that the max observed error reaches 3.8%, approximately.

Figure 11 and Figure 12 show the location of MBF in a 2-dimensional contour graph and the 3-dimensional plot of optimal MBF in terms of current and gas pressure.
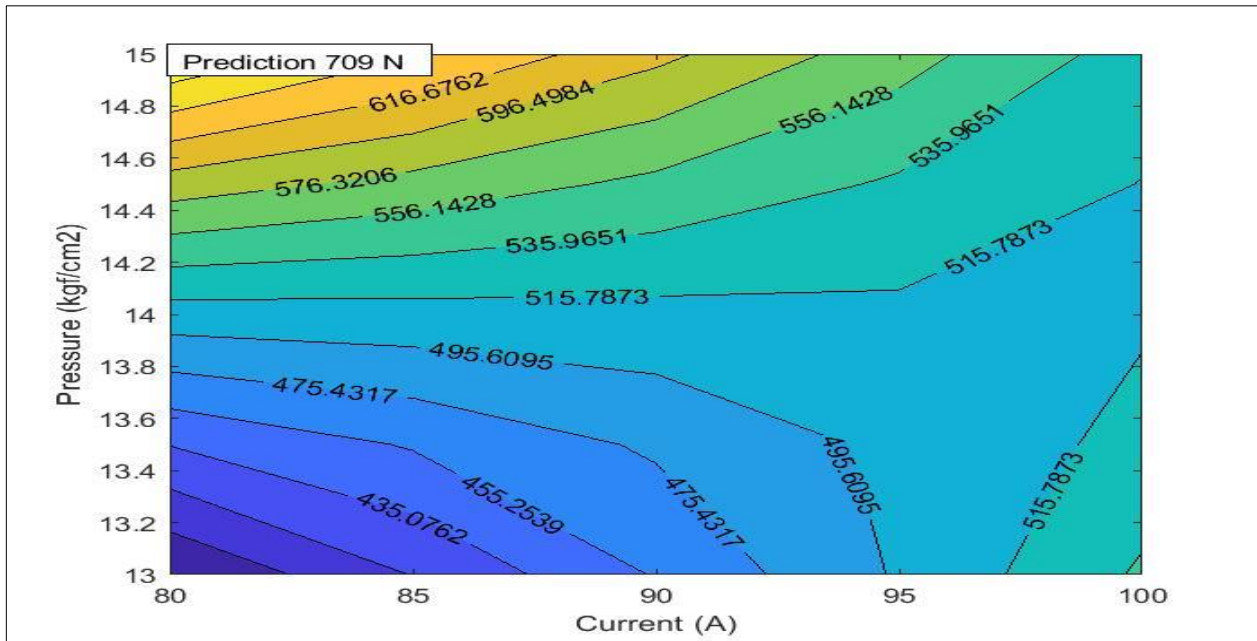
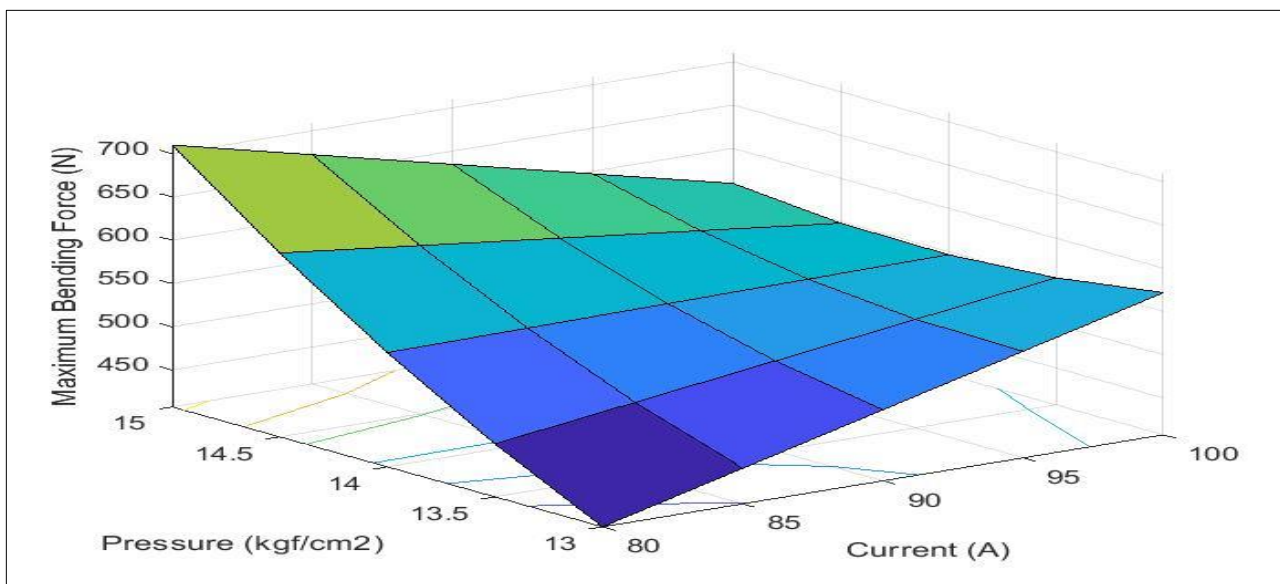Fig 11 2-Dimensional Graph Showing the Location of the Optimal MBF

Fig 12 3-Dimensional Graph of MBF Regarding Gas Pressure and Current Values

Based on these figures, the optimal value of the MBF is obtained from the min weld current level of ($80\ Amp$) and the max gas pressure level of ($15\ Kgf/cm^2$).

V. CONCLUSION

According to both the predicted and experimental findings, the MBF is increased due to increasing the input parameters, which are the current and gas pressure. A higher effect is generated by the gas pressure on the MBF when compared to the current effect. Based on the numerical optimization at a max desirability value of 0.884, the highest recorded value of MBF is $709\ N$ at $15\ Kgf/cm^2$ gas pressure and $80\ Amp$ welding current as optimum values. The confirmation tests confirm an agreement among the predicted (theoretical) and experimental outcomes, with a 3.8% max error value of the MBF. When the welding gas pressure is increased, the tensile strength will also increase. Additionally, the increment in gas pressure and current individually will cause a visual increment in both elongation and yield stress. Moreover, the effect of both parameters generates the minimum values of elongation and yield stress.

REFERENCES

[1]. Babbar, A., Kumar, A., Jain, V. & Gupta, D., 2019. Enhancement of activated tungsten inert gas (A-TIG) welding using multi-component TiO2-SiO2-Al2O3 hybrid flux. *Measurement,* Volume 148.

[2]. ÇALIGÜLÜ , U., CALIGULU, U., DIKBAS, H. & TASKIN, M., 2012. Microstructural Characteristic of Dissimilar Welded Components (AISI 430 Ferritic-AISI 304 Austenitic Stainless Steels) by CO2 Laser

Beam Welding (LBW). *Gazi University Journal of Science,* pp. 25 (1), 35-51.

[3]. Juang, S. C. & Tarng, Y. S., 2002. Process parameter selection for optimizing the weld pool geometry in the tungsten inert gas welding of stainless steel. *Journal of Materials Processing Technology,* pp. 122, (33–37).

[4]. Kesava, R. A., 2021. Investigation on effect of tig welding parameters on dissimilar weld joints of aisi 304 and aisi 310 steels using response surface method. *Sigma Journal of Engineering and Natural Sciences,* pp. 39(1), 80-96.

[5]. Kumar, S. & Shahi, A. S., 2011. Effect of heat input on the microstructure and mechanical properties of gas tungsten arc welded AISI 304 stainless steel joints. *Materials & Design,* pp. 32(6), 3617-3623.

[6]. Kumar, T. S., Balasubramanian, V. & Sanavullah, M. Y., 2007. Influences of pulsed current tungsten inert gas welding parameters on the tensile properties of AA 6061 aluminium alloy. *Materials & Design,* 28(7), pp. 2080-2092.

[7]. Naik, A. B. & Reddy, A. C., 2018. Optimization of tensile strength in TIG welding using the Taguchi method and analysis of variance (ANOVA). *Thermal Science and Engineering Progress,* pp. 8, 327-339.

[8]. Ogedengbe, T. I., Abioye, T. E. & Ekpemogu, A. I., 2018. Investigation of mechanical properties and parametric optimization of the dissimilar GTAW of AISI 304 stainless steel and low carbon steel.. *World Journal of Engineering..*

[9]. Saha, M. K., Hazra, R., Mondal, A. & Das, S., 2019. Effect of Heat Input on Geometry of Austenitic Stainless Steel Weld Bead on Low Carbon Steel. *Journal of The Institution of Engineers (India): Series C,* pp. 100, pages607–615.

[10]. Zuhailawati, H., Jamaluddin, M. A., AbuSeman, A. & Ismail, S., 2016. Welding Investigation and Prediction of Tensile Strength of 304 Stainless Steel Sheet Metal Joint by Response Surface Methodology. *Procedia Chemistry,* pp. 19, 217-221.